WSRC-MS-96-0591

CONF-970726--15

Thermal Stress Analysis of an Am/Cm Stabilization Bushing Melter

by

C. Gong

Westinghouse Savannah River Company
Savannah River Site
Aiken, South Carolina 29808

B. J. Hardy

A document prepared for 1997 ASME PRESSURE VESSEL AND PIPING CONFERENCE at Orlando, FL, USA from 7/27/97 - 7/31/97.

DOE Contract No. **DE-AC09-89SR18035**

DISCLAIMER

THERMAL STRESS ANALYSIS OF AN AM/CM STABILIZATION BUSHING MELTER

Chung Gong
Savannah River Technology Center
Westinghouse Savannah River Company
773-42A, Room 154
Aiken, South Carolina 29808

Telephone: (803) 725-3167
Fax: (803) 725-8829
e-mail: chung.gong@srs.gov

Bruce J. Hardy
Savannah River Technology Center
Westinghouse Savannah River Company
704-1T, Room 232
Aiken, South Carolina 29808

Telephone: (803) 557-7113
Fax: (803) 557-7008
e-mail: bruce.hardy@srs.gov

Decades of nuclear material production at the Savannah River Site (SRS) has resulted in the generation of large quantities of the isotopes Am^{243} and Cm^{244}. Currently, the Am and Cm isotopes are stored as a nitric acid solution in a tank. The Am and Cm isotopes have great commercial value but must be transferred to the Oak Ridge National Laboratory (ORNL) for processing. The nitric acid solution contains other isotopes and is intensely radioactive, which makes storage a problem and precludes shipment in the liquid form. In order to stabilize the material for onsite storage and to permit transport the material from SRS to ORNL, it has been proposed that the Am and Cm be separated from other isotopes in the solution and vitrified.

The vitrification process in the Platinum-Rhodium alloy vessel generates a wide spectrum of temperature distributions. The melter is partially supported by a suspension system and confined by the flexible insulation. The combination of the fluctuation of temperature distribution and variable boundary conditions, induces stresses and strains in the melter. The thermal stress analysis is carried out with the finite element code ABAQUS. This analysis is closely associated with the design, manufacture and testing of the melter. The results were compared with the test data.

THERMAL STRESS ANALYSIS OF AN AM/CM STABILIZATION BUSHING MELTER

Chung Gong
Savannah River Technology Center
Westinghouse Savannah River Company
773-42A, Room 154
Aiken, South Carolina 29808

Bruce J. Hardy
Savannah River Technology Center
Westinghouse Savannah River Company
704-1T, Room 232
Aiken, South Carolina 29808

1. INTRODUCTION

Decades of nuclear material production at the Savannah River Site (SRS) has resulted in the generation of kilogram quantities of the isotopes Am^{243} and Cm^{244}. Currently, the Am and Cm isotopes are stored in a tank as a nitric acid solution. The solution contains other isotopes and is intensely radioactive, which makes long term storage a problem and precludes shipment in the liquid form. The Am and Cm isotopes are not merely waste material, the isotopes have great commercial value but must be transferred to the Oak Ridge National Laboratory (ORNL) for processing. In order to stabilize the material for onsite storage and to transport the material from SRS to ORNL, it has been proposed that the Am and Cm be separated from the majority of the other isotopes in the solution and vitrified.

Vitrification will be effected by depositing a liquid feed stream containing the isotopes in solution, together with a stream of glass frit, onto the top of a molten glass pool in a melter. The glass is non-conducting and the melter is a rectangular vessel composed of platinum/rhodium alloy and which is resistively heated. The majority of the evaporation of water in the liquid feed occurs in the frit bed formed on the surface of the glass pool. The wetted frit bed is called a "cold cap". Because most of the power is required to evaporate the liquid, power demands differ for the upper and lower parts of the melter. In addition, the melter is batch fed so that the power requirements at the top and bottom of the melter vary with time. To vary the fraction of the total power delivered to the upper and lower parts of the melter, pairs of upper and lower electrodes were placed on the melter and connected to variable power supplies.

In order to ensure that the electrode configuration could effectively vary power between the top and bottom of the melter, and to identify regions of high power density, an analysis of the melter power distribution was performed with the ABAQUS® finite element code.

ABAQUS was used to calculate the electric potential and current density distributions in the melter for a variety of current and potential boundary conditions. The results of the calculation were compared with test data and were used to compute power densities for input to a computational fluid dynamics model for the melter.

During melter heat-up, thermal expansion may cause permanent deformation. Further, the melter will operate at temperatures near 1400°C. At these temperatures the melter is entirely in the regime of plastic deformation and the structural integrity and stability of the melter was questioned. The stress and strain in the melter during heat-up and at the operating temperature was estimated from a model based on the ABAQUS code .

This report documents the power distribution and stress calculations performed for Melters 2A and 2B which are to be used in the Am/Cm vitrification program.

2. BACKGROUND

The design of Melters 2A and 2B, is based on operating experience with Melter 1. Melter 1 was a rectangular box with a bottom which sloped toward a central drain tube. Melter 1 was approximately 11 in. tall, 10 in. wide and 2.5 in. deep. The top of the melter had a 2.5 in. by 10 in. rectangular opening. One pair of electrodes was attached on opposite sides of the melter.

Initially, it was believed that Melter 1 could be run as a continuous process. However, operating experience dictated that it was necessary to run in batch mode. During tests with Melter 1, it soon became obvious that the operation of the melter must be divided into three phases; feeding, heating and a pouring. In the feeding phase, inventory is accumulated by depositing nitric acid solution and glass frit on the surface of the glass pool. The majority of the power is used to evaporate the nitric acid solution. Therefore, most of the power must be applied to the top of the melter during the feeding phase . After sufficient inventory is accumulated in the melter, the heating phase begins. In this phase the feed is stopped and the remaining liquid evaporates from the cold cap. The remaining layer of dried frit and crust is heated until it is melted into the glass pool, which is heated until an equilibrium state is reached within the melter. It is believed that the melter may be allowed to idle indefinitely at this state without adversely affecting the product or system. During the heating phase it is believed that it will be necessary to shift power toward the bottom of the melter. After equilibrium has been reached in the heating phase, the glass is ready to

pour. This is the pouring phase. Glass pour is initiated by melting the solid glass in the drain tube with the drain tube heater. It is believed that the power distribution during the pouring phase will need to be uniform or shifted slightly toward the bottom of the melter.

In the Melter 1 tests it was found that radiative losses from the top were sufficiently high that the glass in this region was not completely melted when the plenum was in place. Because of this behavior, Melters 2A and 2B were designed with a partially covered top to direct thermal radiation onto the cold cap rather than allowing it to escape into the plenum. In addition, two pairs of electrodes were attached to Melters 2A and 2B and connected to variable power supplies. The pairs of electrodes are attached to the narrow sides of the melters at the top and bottom, see Figures 1-1 and 1-2. This electrode geometry allows the power to be varied between the top and bottom of the melter as needed for the particular phase of operation.

Excessive thermally induced strain was also a problem with Melter 1. Melter 1 was encased in cast refractory with no allowance for thermal expansion. Further, both the top and bottom of Melter 1 were rigidly fixed, allowing for no vertical expansion. When the melter was heated it expanded against the refractory material, which had a substantially lower coefficient of thermal expansion. In addition, the melter expanded against the rigid top and bottom members. The walls of Melter 1 experienced substantial buckling and a tear was observed. It must be noted however, that the tear may have occurred during attempts to force glassy deposits into the glass pool by pushing against them with a mullite rod. In order to allow for vertical thermal expansion in Melters 2A and 2B, the bottom of the melter was supported on springs. Lateral expansion against the refractory material was accommodated by using fiberfrax (ceramic papers) as a spacer.

3. MELTER GEOMETRY

Melters 2A and 2B are flat, tall rectangular boxes made of platinum-rhodium alloys and were fabricated by GAFtech, Inc. of Nashville, TN. Because differences in the melter configurations are insignificant with regards to power and stress distributions, only one melter model was used for both Melters 2A and 2B . The height of both melters is 11 inches, the width is 10 inches and the depth is 2.75 inches, see Figures 1-1 and 1-2.

There are two pairs of flat electrodes, referred to as "ears", on the short sides of the melter. One pair of ears primarily delivers power to the upper part of the melter while the other pair

of ears primarily supplies power to the bottom. Inside the melter there are two pairs of vertical screens welded to the side walls with the longitudinal axis of the screens traversing the width of the melter. In order to relieve thermal buckling stresses, each of the screens has a cusp like bend at approximately one inch from each end. Additionally, two cross braces (in the form of an X) are attached between the two top screens at a distance of three inches from ends. The middle screens are also cross braced. A flange plate is attached at the top of the melter. The melter is constructed with 0.06 inches thick platinum-rhodium alloys plates except the top flange (including the drain wall) which are made of 0.03 inch thick plates. The ears are 0.188 inches thick.

4. NUMERICAL METHODS

4.1. Method of Analysis

The finite element method was used to numerically model the electrical and mechanical behavior of Melters 2A and 2B. The mesh was generated with the pre-processor, MSC/PATRAN® and the analysis was performed with the ABAQUS® code. The ABAQUS POST post-processor was used to facilitate the post-processing of the results.

4.2. Description of the Pre- and Post-processor

MSC/PATRAN® [MSC/PATRAN, 1996] is a versatile geometric and graphic modeling code developed by PDA Engineering which was acquired by the MacNeal-Schwendler Corporation. The MSC/PATRAN system's ability to interface with a large array of applications is provided by the PATRAN Neutral File, the PATRAN Results File, and the Application Interface. Post-processing of the results was accomplished using ABAQUS POST.

4.3. Main Processor

ABAQUS® [ABAQUS, 1995], is a general purpose finite element analysis program with special emphasis on advanced linear and nonlinear structural engineering, heat transfer as well as coupled thermal-electrical applications. Hibbitt, Karlsson & Sorensen, Inc. (HKS) developed and support this computer code. The ABAQUS version presently in use at SRS (5.5-1N) is marketed by HKS as a "Nuclear QA Grade" code that complies with the NQA-1 quality assurance standard. Details of the Quality Assurance controls for the ABAQUS code may be found in the Technical and QA Plan for ABAQUS.

4.4. Finite Element Modeling

Melters 2A and 2B possess symmetry with respect to two orthogonal planes. In the case of symmetrically applied loads arising from a uniform temperature distribution, a quarter model cut out along the symmetry planes of the melter was sufficient for the analysis. However, in the analysis of the power distribution, the electrical currents flow from the ears on one side of the melter to those on the other side. The current density distribution then reduces the problem to reflective symmetry about the plane through the long cross-section of the melter which contains the four ears.

For the power distribution analysis, ABAQUS requires solid continuum elements in the model. This model will also be used for thermal stress analysis. The melter is constructed with thin plates. Hence, the bending stress as well as the membrane stress are important in the structural integrity analysis, especially at the corners of plate intersections. In order to demonstrate the elastic-plastic bending behavior of a plate at high temperature gradient, at least four elements across the thickness of the plate are needed. Based upon experience, it was found that if there are eight elements across the thickness of the plate the solution will be smoother, especially at those corners. Nevertheless, limited by the capacity of the computer, the current model was meshed with only two elements through the thickness of the plate. If the stresses in the plate are below the yield limit of the material, the two-element approximation will still provide good information about the mechanical behavior of the melter. Previous calculations (modeled with shell elements) indicate that if the melter were heated with uniformly distributed temperature up to 1600 °C, the stresses approach twice the yield limit. At certain regions in the melter, the resolution of the model may be insufficient to obtain accurate stress distribution. However, for the overall stress distribution in the melter, it is valid to use two elements (in the thickness of the plate).

The thinnest plate in the melter is only 0.03 inches thick. In order to maintain a mathematically tolerable aspect ratio, the other dimensions of the elements were less than 0.12 inches (for double elements in the thickness of the plate) so that the aspect ratio was kept below 8. Attempts to maintain a low aspect ratio in the model resulted in an excessive increase in the number of elements. However, through several trial runs, a workable finite element model was developed The average aspect ratio of the elements in the melter was 7.35. Whereas in the top flange, the aspect ratios were higher than 8, and the maximum aspect ratio reached 32. At the normal intersections of the melter plates and screens the elements became smaller. In these dense regions the aspect ratios of the elements were on the order of 56. The total number of solid continuum elements in this model was 12,568 with 20,428 nodes (total number of variables is 40,856).

There were twelve circular holes on each of the top screens. Two sets of double cross-bars were installed to connect each pair of the top and middle screens. The cusps on both ends of each of the screens were also modeled. The finite element mesh is shown in Figure 4-1.

The melter was meshed with 3-D solid continuum elements DC3D8E (8-node linear brick) (C3D8 for stress analysis) in the coupled thermal-electrical analysis with ABAQUS. In a small transition region where the geometry precludes the use of DC3D8E, twelve DC3D6E (6-node linear triangular prism) (C3D6 for stress analysis) elements were implemented.

5. MATERIAL PROPERTIES

Melters 2A and 2B are to be manufactured with platinum-rhodium alloys. Two compositions have been chosen as the primary materials for the melter: 90% platinum 10% rhodium alloy and 80% platinum 20% rhodium alloy.

There is a paucity of material data for platinum-rhodium alloys at the operating temperatures for the melter. The temperature dependent properties of platinum-rhodium alloys are not readily available from usual material handbooks. Material properties of the platinum-rhodium alloys in this study were mostly obtained from two sources, viz., a reference book [Vines, 1941] published by the International Nickel Company and scattered pieces of information obtained from Dr. Louis Toth of Engelhard-Clal [Toth, 1996], who assisted us with our literature search. Many of the high temperature physical properties of the platinum-rhodium alloys were selectively chosen from conflicting data or extrapolated from the limited data available. All the material properties data obtained are converted into the SI system, which constitutes the system of units for this analysis.

5.1. Mass Density

The mass density of the platinum rhodium alloys can be found in References [Toth, 1996, ASM, 1990]. The values listed in Table 5-1 are the mass densities of the alloys at 30°C [ASM, 1990, p. 710, Table 8].

Table 5-1. Mass density of platinum-rhodium alloys

Alloy	Density (kg/m^3)
90% Pt - 10% Rh	19,970
80% Pt - 20% Rh	18,740

5.2. Modulus of Elasticity

In this Table 5-2 the moduli of elasticity for the 90% platinum 10% rhodium alloy and the 70% platinum 30% rhodium alloy are digitized from the curves obtained by applying ultrasonic techniques [Papadakis *et al.*, 1974]. The modulus for the 80% platinum 20% rhodium alloy is computed by averaging the moduli of the neighboring alloys. The Poisson's ratio of a metal usually increases with increasing temperature. The yield limit of a metal decreases with increasing temperature. In the plastic state, most metals are virtually incompressible, i.e., the Poisson's ratio of the material approaches 0.5. With an understanding of the material behaviors and the mathematical modeling of the constitutive relations [Malvern, 1969; ABAQUS, 1995], the Poisson's ratio of the platinum-rhodium alloys is chosen as 0.33 for the range of temperatures in this model.

Table 5-2. The modulus of elasticity for platinum-rhodium alloys

Temperature (°C)	Modulus of Elasticity (MPa)		
	Pt90Rh10	Pt80Rh20	Pt70Rh30
0	193,000	219,500	246,000
50	191,000	217,250	243,500
100	189,000	214,500	240,000
200	185,000	209,990	234,980
300	181,000	205,250	229,500
400	176,000	199,500	223,000
500	171,500	194,250	217,000
600	167,500	188,725	209,950
700	163,000	182,500	202,000
800	157,500	176,750	196,000
900	152,500	171,250	190,000
1000	147,500	165,750	184,000
1100	142,500	159,250	176,000
1200	137,000	153,000	169,000
1300	129,000	144,000	159,000
1400	120,000	135,000	150,000
1500	110,000	125,500	141,000

5.3. Yield Strength and Ultimate Tensile Strength

The characteristic mechanical behavior of platinum-rhodium alloys at elevated temperatures has profound effects in the analysis of the Am/Cm bushing melter. The thermal loading as well as the mechanical loading during the vitrification operation will inflict both geometrical and material nonlinearities upon the melter.

The stress-strain relation of the materials over the full range of the operational temperatures is essential for the nonlinear analysis of the melter. In a nonlinear analysis, the mechanical behavior of the material determines the distribution of stress and strain in the structure. Large deformations of a structure alters the distribution of stiffness, which affects the load bearing capacity of the structure.

Searching for the temperature dependent mechanical properties of the platinum-rhodium alloys is still in progress. A bit of information is provided by Dr. Toth of Engelhard [Toth, 1996]. In the Table "Hot Tensile Strength" of the referenced document, the ultimate tensile strength and elongation of 17 platinum alloys are listed for temperatures range from 500 °C to 1600 °C. According to Dr. Toth, these data are valid for hard worked wires 0.050 inches in diameter. The sample length is 18 inches, whereas the furnace length is 12 inches. The heating time is 5 minutes. The test shows a 75% reduction in the ultimate tensile strength from the last annealing. The data listed in the Table are in the British units. The ultimate tensile strength and elongation for the 90% platinum 10% rhodium and 80% platinum 20% rhodium alloys were converted into SI units. In an analysis with material nonlinearity and/or geometrical nonlinearity, true stress and natural strain should be used in the constitutive equations [Malvern, 1969]. The ultimate tensile strength and elongation which were measured in engineering units were transformed into true and natural measurements for the finite element analysis.

The yield strength of a material in the stress strain curve plays an important role, particularly in the nonlinear analysis. In the elastic state, before reaching the yield limit, the mechanical behavior of the material is essentially linear. Beyond the yield limit the material enters the plastic state. In the plastic region the strength of the material varies with the increase of strain. The stress strain relation is nonlinear. Unfortunately the yield strength as well as the stress strain curve of the platinum alloys are not available in general. For the annealed condition, Dr. Toth [Toth, 1996] provided yield strength data for 7 platinum alloys at room temperature. Without additional references, the best conjecture would be that the ratio of the yield limit to the ultimate tensile strength of an alloy remains constant as the temperature increases. The room temperature ultimate tensile strength of the alloys platinum 10% rhodium and platinum 20% rhodium can be found in [Vines, 1941, Table 41].

With only the yield strength and ultimate tensile strength being provided along a stress strain curve, the curve can be approximated with two straight line segments. The corresponding strains can be computed from the modulus of elasticity and the elongation. That is, the percentage of elongation that is measured at the point of rupture. The ultimate strain is about 80% of the rupture strain. Of course, the ratio of the ultimate strain to the rupture strain varies with alloys and temperatures. The ultimate strains of the annealed alloys may be different from that of the hard worked alloys. In reality, as temperature increases, the metallurgical discrepancy between the hard worked and the annealed alloys diminishes. Without sufficient supporting data to show the difference, the ultimate strains of the hard worked alloys would also be applied to the annealed alloys in this model.

As suggested by Dr. Toth, the yield strength of an alloy is about 20% ~ 25% of its ultimate tensile strength. The yield strength of the annealed platinum 10% rhodium alloy (18.3 ksi) is also within the 20% ~ 25% range of the ultimate tensile strength of the hard worked alloy. Therefore, the provided room temperature yield strength was applied to both hard worked and annealed platinum 10% rhodium alloy. At high temperatures the mechanical behavior of both the hard worked and annealed platinum alloys approach the same plateau. The ultimate tensile strength of the annealed platinum 10% rhodium alloy was found in [Vines, 1941, Table 42]. The bi-linear stress strain relations for the platinum 10% rhodium alloy were converted into SI units and are listed in Tables 5-3 and 5-4 as functions of temperature.

The temperature dependent ultimate tensile strength of the 80% platinum 20% rhodium alloy was directly converted from a table provided by Toth [Toth, 1996]. However, the yield strength for the annealed alloy could not be adopted for the hard worked 80% platinum 20% rhodium alloy. The room temperature ultimate tensile strength of the 80% platinum 20% rhodium alloy was quoted from [Vines, 1941, Table 41]. The yield limit of the alloy is taken as 20% of the ultimate tensile strength. Then the yield strength and the ultimate tensile strength of the hard worked 80% platinum 20% rhodium alloy were listed as functions of temperature in Table 5-5.

Table 5-3. The yield strength and ultimate tensile strength of hard worked 90% platinum 10% rhodium alloy

Temperature (°C)	Yield Strength (MPa)	Ultimate Tensile Strength (MPa)	Natural Strain (%)
20	1.261748E+02	6.267373E+02	7.968170E-01
500	1.051457E+02	5.326233E+02	2.371653E+00
600	9.154686E+01	4.817466E+02	5.448819E+00
700	7.864898E+01	4.293461E+02	8.434115E+00
800	6.505014E+01	3.679065E+02	1.133287E+01
900	3.252507E+01	2.319411E+02	3.074847E+01
1000	2.004778E+01	1.607109E+02	4.081282E+01
1100	1.710370E+01	1.387923E+02	4.187103E+01
1200	1.640273E+01	1.331041E+02	4.187103E+01
1300	1.401943E+01	1.137642E+02	4.187103E+01
1400	1.093515E+01	8.873608E+01	4.187103E+01
1500	9.252822E+00	7.508437E+01	4.187103E+01
1600	7.850879E+00	5.559967E+01	3.015850E+01

Table 5-4. The yield strength and ultimate tensile strength of the annealed 90% platinum 10% rhodium alloy

Temperature (°C)	Yield Strength (MPa)	Ultimate Tensile Strength (MPa)	Natural Strain (%)
20	1.261748E+02	3.342599E+02	7.968170E-01
500	8.411656E+01	2.272526E+02	2.371653E+00
700	6.834471E+01	1.989839E+02	8.434115E+00
900	4.731557E+01	1.799543E+02	3.074847E+01
1100	2.812647E+01	1.217277E+02	4.187103E+01
1300	2.050341E+01	8.873608E+01	4.187103E+01
1500	1.472040E+01	6.370795E+01	4.187103E+01

Table 5-5. The yield strength and ultimate tensile strength of the hard worked 80% platinum 20% rhodium alloy

Temperature (°C)	Yield Strength (MPa)	Ultimate Tensile Strength (MPa)	Natural Strain (%)
20	1.792648E+02	9.106652E+02	1.587335E+00
500	1.294843E+02	6.629598E+02	2.371653E+00
600	9.638930E+01	4.935132E+02	2.371653E+00
700	1.012157E+02	5.141756E+02	1.587335E+00
800	8.577131E+01	4.460108E+02	3.922071E+00
900	5.833001E+01	3.103156E+02	6.203539E+00
1000	3.378452E+01	2.297347E+02	3.074847E+01
1100	2.385601E+01	1.612666E+02	3.015850E+01
1200	2.109809E+01	1.434670E+02	3.074847E+01
1300	1.751279E+01	1.113814E+02	2.405905E+01
1400	1.475487E+01	9.443118E+01	2.468601E+01
1500	1.130747E+01	8.277070E+01	3.811724E+01
1600	9.101136E+00	6.443604E+01	3.478360E+01

The ultimate tensile strength of annealed 80% platinum 20% rhodium alloy at room temperature can be found in [Vines, 1941, Table 41]. The yield strength is given in [Toth, 1996] . Nevertheless, the variation of the ultimate tensile strength and yield strength as a function of temperature is still unknown. The yield strength and the ultimate tensile strength of annealed 80% platinum 20% rhodium alloy as a function of temperature are listed in Table 5-6. It should be noted that these values are applied under the assumption that the strength ratios between the annealed and the hard worked alloy did not vary with increasing temperature

Table 5-6 The yield strength and ultimate tensile strength of the annealed 80% platinum 20% rhodium alloy

Temperature (°C)	Yield Strength (MPa)	Ultimate Tensile Strength (MPa)	Natural Strain (%)
20	1.206590E+02	4.903582E+02	1.587335E+00
500	8.715292E+01	3.569784E+02	2.371653E+00
600	6.487742E+01	2.657379E+02	2.371653E+00
700	6.812593E+01	2.768638E+02	1.587335E+00
800	5.773069E+01	2.401597E+02	3.922071E+00
900	3.926058E+01	1.670930E+02	6.203539E+00
1000	2.273958E+01	1.237033E+02	3.074847E+01
1100	1.605693E+01	8.683587E+01	3.015850E+01
1200	1.420064E+01	7.725146E+01	3.074847E+01
1300	1.178746E+01	5.997458E+01	2.405905E+01
1400	9.931164E+00	5.084756E+01	2.468601E+01
1500	7.610798E+00	4.456884E+01	3.811724E+01
1600	6.125765E+00	3.469633E+01	3.478360E+01

5.4. Thermal Conductivity

In view of the fact that platinum-rhodium alloys are used extensively for high temperature applications, it is somewhat surprising that the thermal properties of platinum-rhodium alloys are particularly scarce. Insofar as the authors could discern, the specific heat data for the alloys are simply not available. Only a few experimentally obtained values for thermal conductivity could be found for two different of platinum rhodium alloys, namely, 87% platinum 13% rhodium and the 60% platinum-40% rhodium. Test data for the 87% platinum-13% rhodium alloy was fitted with least squares into a simple formula [Mølgaard, 1968]:

$$K_{PR} = 60.7 - 9.2\ (10^3/T) \qquad (5\text{-}1)$$

where: K_{PR} = thermal conductivity of the 87% platinum-13% rhodium alloy in W / K m
T = temperature in K.

The test data for the 60% platinum-40% rhodium alloy was provided by Dr. Louis Toth [Toth, 1996]. The thermal conductivity as a function of temperature is listed in Table 5-7.

Table 5-7. Thermal conductivity of the 60% platinum 40% rhodium alloy

Temperature K	Temperature °C	Thermal Conductivity Cal/sec/cm/K	Thermal Conductivity Watt/M K
250	-23.15	0.105	43.97
400	126.85	0.120	50.25
600	326.85	0.140	58.63
800	526.85	0.155	64.91
1000	726.85	0.165	69.10
1200	926.85	0.172	72.03
1400	1126.85	0.180	75.38
1600	1326.85	0.182	76.21
1800	1526.85	0.187	78.31

5-5. Thermal Expansion Coefficients

The linear thermal expansion ratios (i.e., the ratio of the expanded length to the undeformed length, (L_t / L_o)) were provided by Dr. Toth [Toth, 1996, Table VIII]. The coefficients of thermal expansion were then computed from the linear thermal expansion ratios as listed in Table 5-8.

Table 5-8. The Coefficients of Thermal Expansion for Platinum Rhodium Alloys

Temperature °C	Thermal Expansion Coefficient			
	Pt (90%)-Rh(10%)		Pt (80%)-Rh(20%)	
	L_t/L_o- 1.0	Strain/K	L_t/L_o- 1.0	Strain/K
0	0	0.00000000E+00	0	0.00000000E+00
100	0.001	1.00000000E-05	0.00063	6.30000000E-06
200	0.002	1.00000000E-05	0.0014	7.00000000E-06
300	0.003	1.00000000E-05	0.0023	7.66666667E-06
400	0.0041	1.02500000E-05	0.0032	8.00000000E-06
500	0.0051	1.02000000E-05	0.0043	8.60000000E-06
600	0.0061	1.01666667E-05	0.0053	8.83333333E-06
700	0.0072	1.02857143E-05	0.0063	9.00000000E-06
800	0.0083	1.03750000E-05	0.0075	9.37500000E-06
900	0.0094	1.04444444E-05	0.0087	9.66666667E-06
1000	0.0106	1.06000000E-05	0.0099	9.90000000E-06
1100	0.0117	1.06363636E-05	0.0112	1.01818182E-05
1200	0.0131	1.09166667E-05	0.0125	1.04166667E-05
1300	0.0144	1.10769231E-05	0.0138	1.06153846E-05
1400	0.0158	1.12857143E-05	0.0152	1.08571429E-05
1500	0.0176	1.17333333E-05	0.0167	1.11333333E-05

6. MODEL DESCRIPTION

This study covers three major fields of physics, namely, heat transfer, electrical conduction and continuum mechanics. The three fields are coupled in this analysis. The effect of temperature in all the properties of the materials is conspicuously appreciable in testing, for instance, the Thomson effect [Jones, 1956] that shows the coupling of thermal and electrical currents in power distribution. Whereas the other factors, such as electrical potential gradients, deformation of the element (the Bardeen and Shockley effect), etc. may also alter the properties of the medium. But the changes in material properties due to factors other than temperature are not significant in this analysis.

7. STRESS-STRAIN ANALYSIS

Because of the exigency of this project and the lack of complete material data, a series of preliminary models of the melter were constructed. Although the assumption of a uniform temperature distribution was a reasonable first approximation for the power distribution model, the approximation may not be conservative for the stress-strain model. The reason for this difference is that temperature variations result in non-uniform thermal expansion, which may result in significant stress concentrations in the melter. However, because an accurate thermal model has not been developed at the time of this report, the stress analyses assume a uniform temperature distribution in the entire melter.

In a series of preliminary stress strain analyses, the melter is modeled with shell elements which are mechanically preferred for thin fabrication members. However, for the coupled thermal-electrical analysis, ABAQUS requires 3-D solid continuum elements. For consistency, the stress analysis also performed for the 3-D solid continuum model.

In the preliminary studies, the stress-strain analysis of Melters 2A and 2B assumed that the platinum-rhodium alloy was at a uniform temperature 1600° C. The molten glass was modeled as an inviscid fluid which applied hydrostatic pressure to the walls of the melter. The preliminary studies indicate that the effect of the glass pressure is negligible. Hence in the ensuing analyses, the weight of the glass is not included.

The metler is installed with many different auxiliary parts for various purposes. Each part added to the melter will have a particular thermal mechanical effect in the thermal stress analysis. For some of the insulation components the temperature dependent thermal mechanical properties are not available. To include all the auxiliary parts into the finite element model will excessively increase the number of elements. In the thermal stress

analysis, the main purpose is to determine the mechanical (stress and strain) detriments that inflict upon the melter during the vitrification operation. As the temperature in the melter increases steadily, the physical confinement provided by the surrounding attachments which limit the expansion of the melter, is much more important than the mechanical properties of the constrain materials (such as the insulation devices, etc.). Therefore, a mechanically equivalent confinement device in the numerical process which provide the boundary conditions to the melter will be adequate for this analysis.

Around the melter exterior surfaces, a layer of 0.125 inches (0.003175 meter) thick ceramic paper (3000 AL-4) is inserted between the melter and the fiber-boards. At the bottom of the melter, the melter is insulated with KAST-O-LITE 30 CASTABLE Refractory (mixed with hollow alumina spheres). The casted refractory is supported by four springs. The spring constant of each of the springs is 1,453.5457 Newton/Meter. Each of the springs is guided by a steel rod that allows only vertical motion.

For the confinements surrounding the melter, the finite element model simulates with rigid surfaces. A gap is allowed between the melter exterior surface and the rigid surface. The ceramic paper is not compressed when it is installed. The allowable contraction of the ceramic paper used in this analysis is 0.001 meter which is fairly conservative. At the bottom of the melter, there is no ceramic paper. The refractory is considerably hard as compared with the melter at high temperature. No gap is provided between the bottom surface of the melter and the rigid surface. However, the bottom rigid surface is supported by four mechanical springs. Each of the springs has a spring constant equal to 1,453.5457 Newton/Meter.

Of course, the thermal stress analysis for various temperature gradient distributions in the melter is important. In reality, since the thickness of the melter walls is fairly thin (0.06 inches or 0.001524 meter) and the electrical power distribution in the melter is essentially uniform, the magnitude of temperature gradient will be insignificant. The existence of the temperature gradient in the melter will be transient. At the steady operation temperature, the whole melter may be heated up to 1450 °C.

The finite element analysis of the quarter model of the melter is carried out on the CRAY J916 at SRS. The calculation took 65.83 CPU hours (76.19 hours wall clock time) in 130 calculation increments. At high temperature the melter walls are structurally weak that will cause structural as well as numerical instability. The temperature increment in the

calculation was reduced to less than 0.071 °C during the convergence iteration when the temperature of the melter reached 752.55 °C. Through the calculation, 950 iterations were performed.

During the gradual temperature increasing the whole melter expands uniformly without distortion, until the temperature reaches 752.55 °C. At this temperature, the two narrow end walls are squeezed horizontally against the rigid boundary surfaces. Vertically, the bottom of the melter moves 0.00222 meter down and thus compresses the support spring. The large side plate that is under in-plane compression, remains virtually flat. The large side plate moves outward along the normal to the plate by 0.0003 meter. The screens deflects slightly. Perceptibly, the whole melter is at the verge of structural instability. Mathematically, it implies that the tangential stiffness of the system approaches singularity. In the structural system, a majority part of the degrees of freedom simultaneously coalesce to their bifurcation points. That explains why in this temperature range the incremental temperature is so small for convergence of the solution.

For a linear elastic analysis, the temperature, 752.55 °C is the critical temperature for this structural system. However, in this nonlinear elastic-plastic analysis, the calculation continued passing the massive bifurcation points. Also in this calculation, the stiffness of the system did not completely vanish at the pseudo-critical temperature. As the temperature increases, the flat plates in the melter start to bend.

The melter is fabricated with thin plates and shells. Limited by the size and precision of the computer, the thin plates and shells are modeled with only two elements in the thickness. In the linear elastic state, the bending capacity of a thin plate with two elements in the thickness is reduced approximately by a quarter of its full strength . Whereas in the plastic state, the distinction of the strength of a plate with two elements in the thickness and that of a plate computed with analytic approach will vanish. As a consequence, the thermal mechanical results obtained in this analysis are slightly conservative. The true critical temperature should be higher than 752.55 °C. In the plastic region, the computed deformation and stresses are fairly reliable.

In the temperature range from 758 °C to 912 °C, the large side plate bends outward. The maximum displacement begins at the center of the plate. The region of large outward displacement gradually expands and moves upward as temperature increases. The narrow end walls are braced with the thick ears and the power screens shows little or no

deformation in the beginning. The part of the wall where there is no lateral supports starts to cave in as the temperature reaches 764 °C. The hood starts to twist and the bottom of the melter warps slightly when temperature rises to 777 °C. Eventually, a portion of the large side plate touches the rigid boundary surface by the end of this temperature range. For temperatures above 912 °C, the large side plate reverses its bending curvature and bends concavely outward. That is that the center region of the side plate bends toward the interior of the melter (by 0.0033827 meter). Meanwhile, the center section of the middle screen moves toward the side plate (by 0.0027675 meter) at 1450 °C. The undeformed clearance between the side plate and the screen is 0.017526 meter. The cross-bar bracings between the pair of screens indeed prevent the members from touching each other.

Except at those plate junctions (such as large side plate, narrow end walls and bottom plate; the top flange, hood and the dome connections) where the maximum strains reaches 2.0%, over the entire melter the distribution of the strains is fairly uniform and the maximum magnitude remains in the neighborhood of 1.0% throughout the calculation temperature range. The accumulated thermal strains in the melter are well below the ultimate natural strains at the corresponding temperature levels.

Along the plate junctions the melter is yield plastically at elevated temperatures (above 752.55 °C). However, the maximum von Mises stress in the melter is far below the ultimate tensile strength at the corresponding temperature. The melter may show insignificant permanent deformation in the plate junctions. The melter padded with the flexible ceramic papers has sufficient space for thermal expansion. Some distortion may be found in the top flange and hood connection region.

8. CONCLUSIONS

The melter 2A is fabricated with 90% platinum 10% rhodium alloy thin plates and shells. The melter is practically vulnerable to thermal expansions. Nevertheless, with flexible ceramic papers wrapped around side walls and spring supports at the bottom, the melter is capable to sustain the uniform temperature over the whole melter up to 1450 °C. Through the vitrification processes, of course, local temperature gradient in the melter is unavoidable. Stress concentrations can be found in those high temperature gradient areas. The platinum alloy is a good heat conductor and the plates used in the fabrication are considerably thin (0.03 to 0.06 inches). Therefore the temperature gradients, if exist, in the melter will be insubstantial.

The information contained in this article was developed during the course of work under Contract No. DE-AC09-89SR18035 with the U. S. Department of Energy. By acceptance of this paper, the publisher and/or recipient acknowledges the U. S. Government's right to retain a non-exclusive, royalty-free license in and to any copyright covering this paper along with the right to reproduce, and to authorize others to reproduce all or part of the copyrighted paper.

REFERENCES

ABAQUS® (version 5.5-1N), 1995, *ABAQUS Theory Manual,* Hibbitt, Karlsson & Sorensen, Inc. 1080 Main Street, Pawtucket, RI 02860-4847.

APGreen, 1992, KAST-O-LITE® 30, A. P. Green, Industries, Inc., Mexico, Missouri, 65265, Tel., 314-473-3626, Fax, 314-473-3330.

ASM, 1990, *Metals Handbook,* tenth edition, volume 2, ASM International Handbook Committee.

Jones, H., 1956, "Theory of Electrical and Thermal Conductivity in Metals", in *Handbuch der Physik* (*Encyclopedia of Physics*), vol. XIX, *Electrical Conductivity I*, Edited by S. Flügge, Springer-Verlag, Berlin.

Malvern, L. E., 1969, *Introduction to the Mechanics of a Continuous Medium,* Prentice-Hall, Inc., Englewood Cliffs, New Jersey.

Mølgaard, J., and Smeltzer, W. W., 1968, "The thermal conductivity of 87% platinum - 13% rhodium alloy", Short Communications, *Journal of the Less-Common Metals, 16* (1968) pp. 275~278.

MSC/PATRAN® (version 5.0), 1996, *Installation & Operations Manual,* The MacNeal-Schwendler Corporation, 815 Colorado Boulevard, Los Angeles, CA 90041.

Özisik, M. N., 1985, *HEAT TRANSFER, A Basic Approach,* McGraw-Hill Book Company, New York.

Papadakis, E. P., Fowler, K. A., Lynnworth, L. C., Robertson, A., and Zysk, E. D., 1974, "Ultrasonic measurements of Young's modulus and extensional wave attenuation in refractory metal wires at elevated temperatures with application to ultrasonic thermometry", *Journal of Applied Physics,* Vol. 45, No. 6, June 1974. pp. 2409~2420.

Toth, Louis, 1996, *Private communications* ENGELHARD-CLAL, LP, 700 Blair Road, Carteret, New Jersey 07008, Telephone (908) 205-5870, Fax phone (908) 205-7476.

Vines R. F., 1941, *The Platinum Metals and Their Alloys,* Edited by E. M. Wise, The International Nickel Company, Inc., New York.

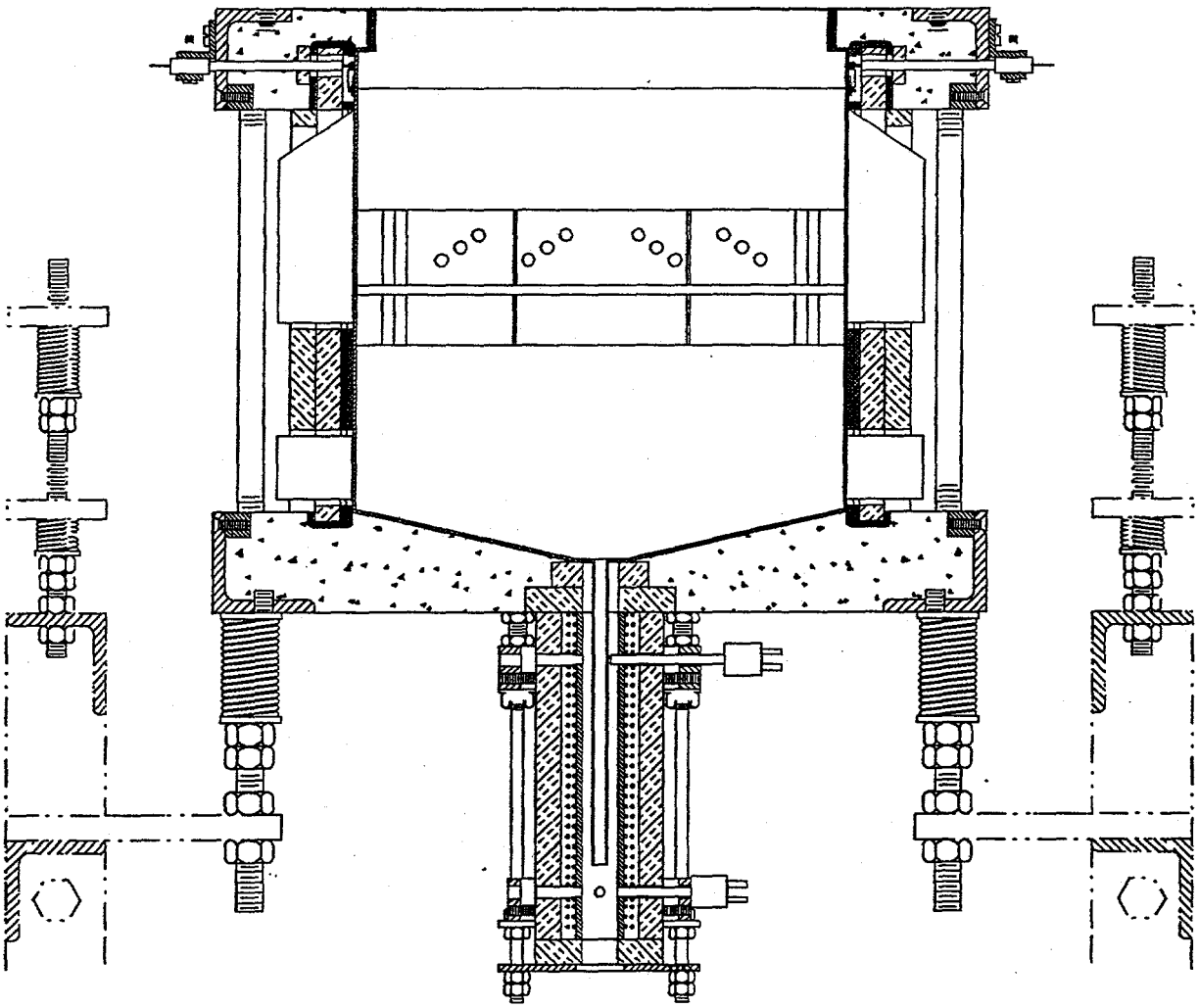

Figure 1-1. Americium/Curium Vitrification Bushing Melter 2A
Middle Plane Section View

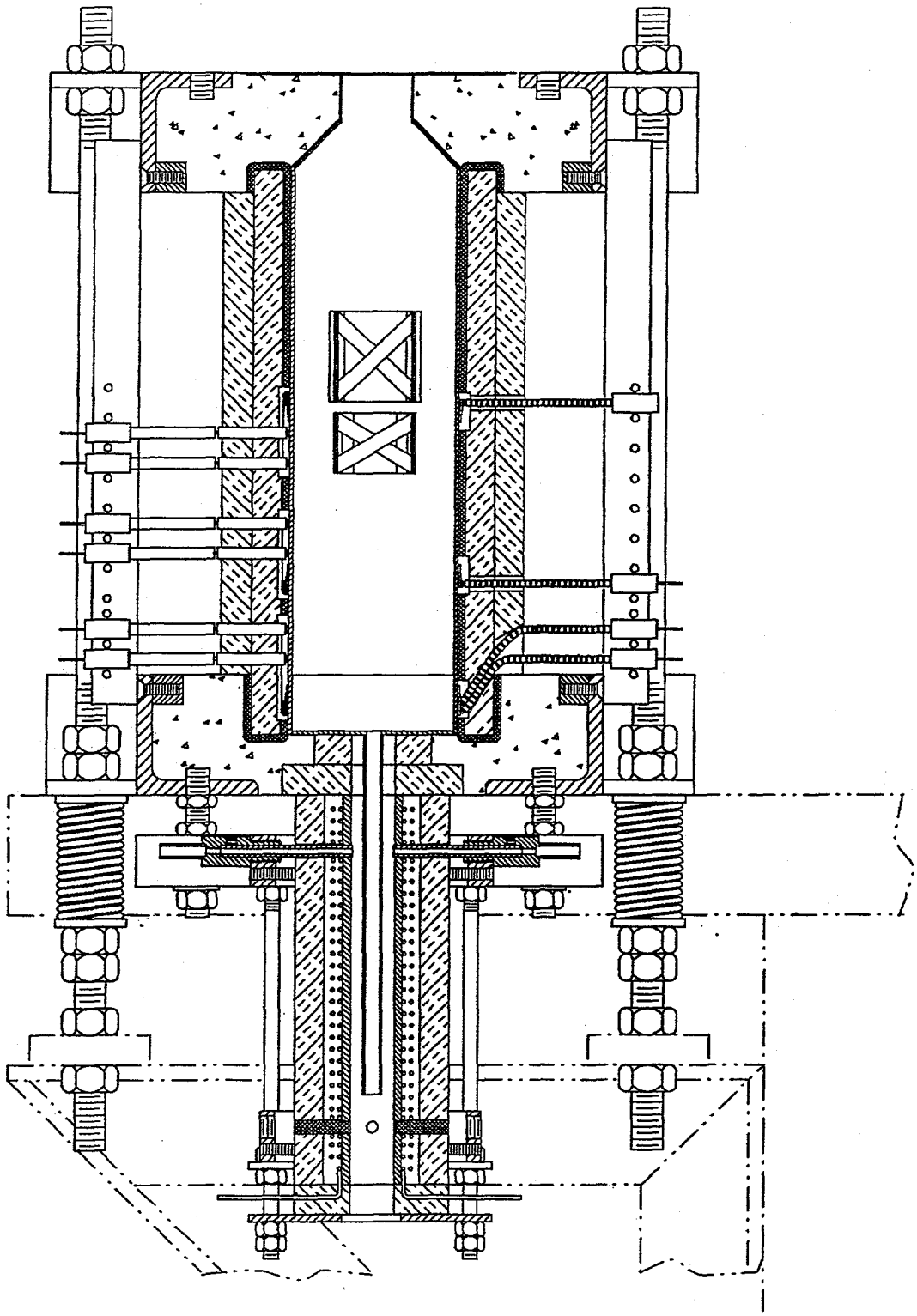

Figure 1-2. Americium/Curium Vitrification Bushing Melter 2A
Side Plane Section View

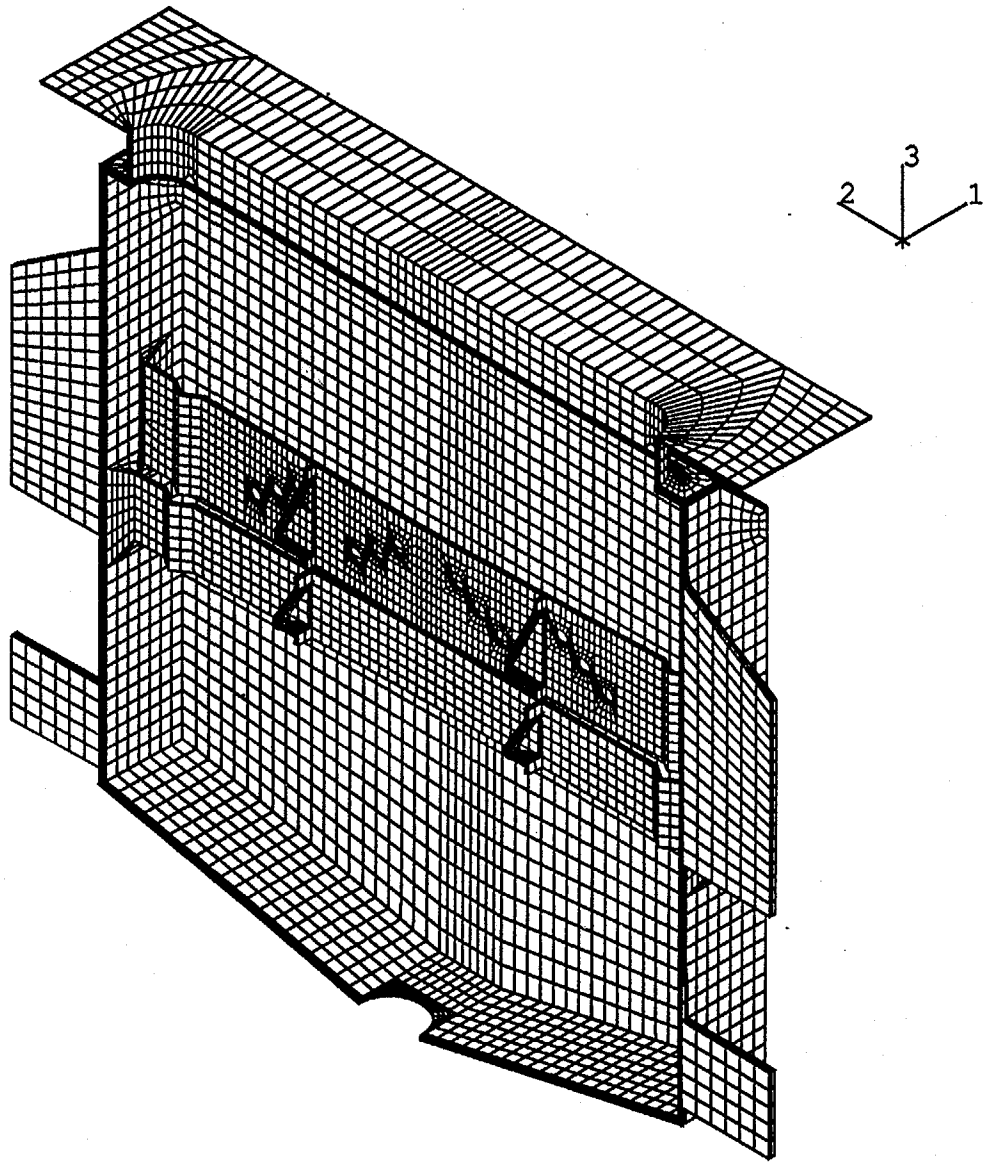

Figure 4-1. Americium/Curium Vitrification Bushing Melter 2A
Finite Element Analysis Mesh